# Understanding How Nanoparticle Attachment Enhances Phosphotriesterase Kinetic Efficiency

Joyce C. Breger,[†,⊥,#] Mario G. Ancona,[§,#] Scott A. Walper,[†] Eunkeu Oh,[‡,||] Kimihiro Susumu,[‡,||] Michael H. Stewart,[‡] Jeffrey R. Deschamps,[†] and Igor L. Medintz*[,†,#]

[†]Center for Bio/Molecular Science and Engineering, Code 6900, [‡]Optical Sciences Division, Code 5600, [§]Electronic Science and Technology Division, Code 6800, U.S. Naval Research Laboratory, Washington, DC 20375, United States, [||]Sotera Defense Solutions, Inc. 7230 Lee DeForest Drive, Columbia, Maryland 21046, United States, and [⊥]American Society for Engineering Education, Washington, DC 20036, United States. [#]These authors contributed equally.,

ABSTRACT As a specific example of the enhancement of enzymatic activity that can be induced by nanoparticles, we investigate the hydrolysis of the organophosphate paraoxon by phosphotriesterase (PTE) when the latter is displayed on semiconductor quantum dots (QDs). PTE conjugation to QDs underwent extensive characterization including structural simulations, electrophoretic mobility shift assays, and dynamic light scattering to confirm orientational and ratiometric control over enzyme display which appears to be necessary for enhancement. PTE hydrolytic activity was then examined when attached to *ca.* 4 and 9 nm diameter QDs in comparison to controls of freely diffusing enzyme alone. The results confirm that the activity of the QD conjugates significantly exceeded that of freely diffusing PTE in both initial rate (∼4-fold) and enzymatic efficiency (∼2-fold). To probe kinetic acceleration, various modified assays including those with increased temperature, presence of a competitive inhibitor, and increased viscosity were undertaken to measure the activation energy and dissociation rates. Cumulatively, the data indicate that the higher activity is due to an acceleration in enzyme−product dissociation that is presumably driven by the markedly different microenvironment of the PTE-QD bioconjugate's hydration layer. This report highlights how a specific change in an enzymatic mechanism can be both identified and directly linked to its enhanced activity when displayed on a nanoparticle. Moreover, the generality of the mechanism suggests that it could well be responsible for other examples of nanoparticle-enhanced catalysis.
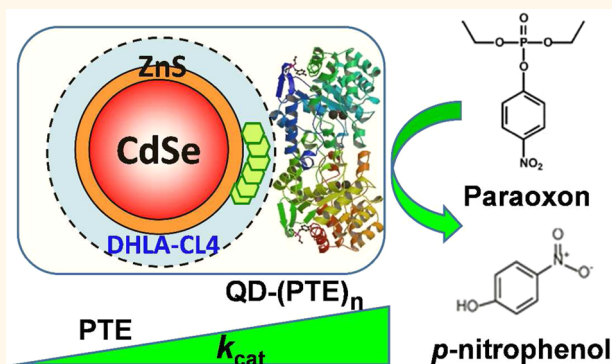
Because of their breadth of applicability and specificity of action, enzymes are the crucial enabler for a wide and growing spectrum of biotechnological applications including recombinant molecular biology, biosynthesis, fuel and food production/processing, sensors, diagnostics, bioremediation, and pharmaceuticals.[1−9] This expanded use is driving related research areas with a focus on increasing enzyme activity, stability, yield, and choice of substrate using mutagenesis and selection technologies.[10] Such approaches are often frustrated by the need to maintain the enzyme's catalytic site essentially unaltered.[9,11] In contrast to the goal of synthetic biology, wherein the enzyme acts within the native cellular metabolism,[2,12,13] many applications seek to exploit an individual enzyme's capabilities *ex vivo*, and in essence incorporate just the protein and its targeted activity within a desired process. This latter utility is itself complicated by issues of metastability, and so enzymes are commonly immobilized on surfaces or porous media which, in many cases, is found to degrade activity.[14−17] Implicated in this loss of function are a number of factors including heterogeneous attachment chemistry which gives rise to mixed avidity, altered diffusion kinetics and repulsion near a bulk surface, issues of steric hindrance and binding site accessibility, along with constraints on enzyme movement which limits the ability of the enzyme

to "sample" the substrate and find the binding conformation needed for catalysis.[14−18] A growing body of evidence, however, suggests that these factors can be suppressed and/or overcome when the enzymes (or substrates) are attached to nanoparticles (NPs) so as to produce enhanced activity. With this as motivation, the present study examines a specific example of NP-enabled catalytic acceleration with the hope that the general phenomenon might become better understood.

Examples of enhanced enzymatic activity in this context are not limited to a particular class of enzyme or a specific type of nanoparticulate material.[19,20] For example, Konwarh immobilized keratinase on 5−17 nm diameter magnetic Fe_2O_3 NPs and found a >3-fold improvement in specific activity.[21] Puentes attached rhamnulose-1-phosphate aldolase to 47 nm diameter gold nanoparticles (AuNPs) and observed a >4-fold improvement in enzyme activity.[22] Palocci attached lipase to 300 nm poly(methyl methacrylate) (PMMA) NPs and increased the transesterification yield of (±)-1-phenylethanol with vinylacetate almost 2.5 times *versus* free enzyme.[23] In an example of the converse substrate-on-NP configuration, Noble showed that an *N*-acetylglucosamine-capped glycolipid underwent significantly higher rates of enzymatic galactosylation by bovine (1,4)-galactosyltransferase when the glycolipid formed lipid microdomains in ∼800 nm large unilamellar vesicles.[24] Estimated K_m values improved more than 5-fold in this system. Similarly, ribonuclease H activity more than doubled when acting on 13 nm AuNPs displaying a high density of DNA that was complexed with the target mRNA substrate.[25] The potential ramifications of exploiting this type of phenomena mechanistically are epitomized by Smith who showed that physisorbing cellulase on NPs for inclusion within simultaneous saccharification and fermentation reactions provided a 2-fold increase in overall ethanol output.[26]

Our initial work in this area also probed both the substrate-on-NP and enzyme-on-NP configurations. Utilizing a system where semiconductor quantum dot (QD) donors were ratiometrically self-assembled with an acceptor dye-labeled peptide substrate, we investigated trypsin activity at this NP interface.[27] Changes in Förster resonance energy transfer (FRET) following trypsin-catalyzed proteolysis of the QD-displayed peptide were converted into units of enzymatic activity and compared to that of a freely diffusing enzyme–substrate system. With the use of progress curves (*i.e.*, with fixed substrate and variable enzyme concentrations) and an integrated version of the Michaelis–Menten (MM) equation that is better suited to this type of format where NP–substrate concentration is limited, it was observed that enzymatic efficiency (k_{cat}/K_m) was improved by ∼5 times when acting on the NP–substrate complex. Moreover, a "hopping" mode

of proteolysis was identified wherein the trypsin complexes with the NP–substrate and consumes all the available peptide substrate on a given NP before diffusing away and encountering the next NP.[27] This enhancement mechanism has recently been confirmed with several other proteolytic substrates attached to QDs.[28] In the converse configuration, we immobilized the ∼100 kDa enzyme alkaline phosphatase on similar QDs and found a modest but statistically significant increase in enzymatic activity when displayed around the QDs; this occurred despite the fact that this enzyme already functions at the substrate diffusion limit in bulk solution.[29] This system also allowed us to demonstrate a general equivalency between the conventional excess-substrate enzymatic assay and progress curves within the specific context of NP-attached enzymes.

Clearly, far more research is needed to allow enhanced enzymatic activity at a NP interface to evolve from what is essentially a "black-box" phenomena to a predictable and replicable process that can be fully exploited. Here, we contribute to this effort by examining the activity of phosphotriesterase (PTE) when it is attached to two different sizes of QD nanocrystals. We began by characterizing PTE conjugation to the QDs *via* metal-affinity coordination to confirm control over orientation and ratio which is often critical for achieving and demonstrating enhanced activity. PTE catalysis when attached to the QDs confirmed significant enhancement of activity as compared with the free enzyme. Further data collected from modified assay formats suggest that the enhancement originates from a significant increase in the rate of enzyme–product dissociation, and that this uniquely arises from the enzyme's immediate microenvironment on the QD surface. To the best of our knowledge, this represents the first example where changes in a specific enzymatic process can be directly correlated with significant enhancement of enzyme activity when attached to a NP.

RESULTS

Phosphotriesterase, Quantum Dots, Conjugate Self-Assembly, and Enzymatic Assays. PTE's (EC 3.1.8.1) are a family of functionally analogous enzymes that catalyze the hydrolysis of organophosphate ester compounds that have a phosphate center with three surrounding O-linked groups such as the insecticide paraoxon along with structurally similar nerve agents including sarin and tabun that display chiral (thio)phosphonate groups.[30−32] Although a naturally occurring substrate has yet to be identified, it is speculated that PTE activity originated from a lactonase-type enzymatic function.[31] Among the many different structural variants of the enzyme which display some substrate promiscuity, there are similarities in their activity.[30−32] All require a divalent metal which interacts with the substrate to
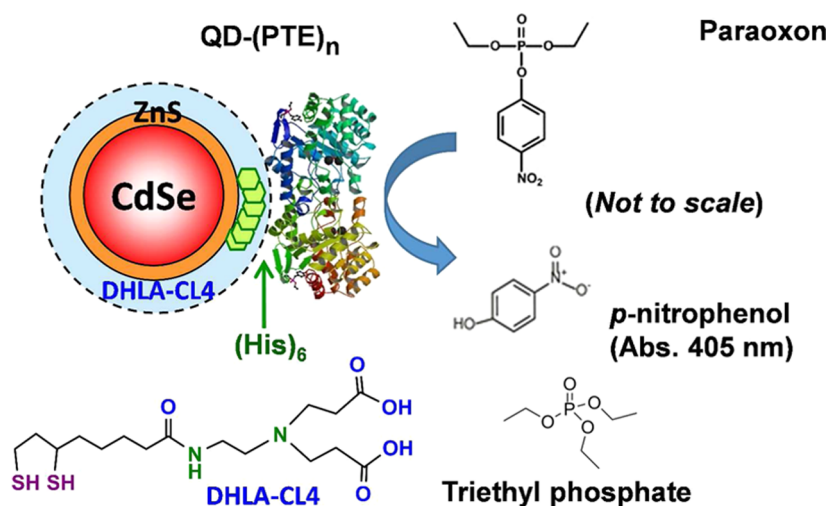
Figure 1. QD phosphotriesterase bioconjugate and paraoxon hydrolysis. Schematic of a CdSe/ZnS core/shell QD surface-functionalized with the DHLA-CL4 ligand whose structure is provided above. PTE is ratiometrically self-assembled to the QD surface by its terminal hexahistidine (His)$_6$ sequence. The average number of PTE per QD is controlled through the molar stoichiometry added during assembly and the conjugates are directly utilized without subsequent purification. PTE hydrolysis of paraoxon substrate to p-nitrophenol product, which absorbs at 405 nm, is also shown schematically. Structure of the PTE competitive inhibitor triethyl phosphate is also provided. Note, not to scale.

facilitate the catalytic step.[33] The hydrophobic substrate binding sites have 3 pockets where 2 of the substituents interact to position the phosphorus center while the last pocket accommodates the leaving group. The actual catalytic step itself is believed to differ mechanistically among enzyme variants. The version utilized here was described by Raushel and colleagues in ref 31 and originates from *Brevundimonas diminuta* (previously called *Pseudomonas diminuta*). The PTE gene lacking the leader sequence and appended with a C-terminal hexahistidine tag was expressed from a plasmid in the *Escherichia coli* BL21(DE3) strain.[34] The 341 residue protein (MW ~37 kDa/net charge of −3 at pH 8.6) forms an obligate dimer with each of the subunits containing a binuclear zinc center that participates in the catalysis.

The two CdSe/ZnS core/shell QDs utilized here consist of green 525 nm and red 625 nm emitting colloidal dispersions as described previously.[29,35,36] For transfer to aqueous phase, the QDs were cap-exchanged with a compact zwitterionic dihydrolipoic acid derivative referred to as DHLA-CL4, see Figure 1. The ligand's bidentate thiols provide for strong binding to the QD surface, while the zwitterionic moiety provides broad pH and ionic colloidal stability despite the fact that the molecules overall size is among the smallest available for QD functionalization and contributes minimally to the hydrodynamic diameter (D_H) of the dispersed nanocrystals.[36] The long-term stability of QD materials prepared with this ligand have been repeatedly confirmed in a variety of challenging biological environments.[37−41] More importantly, this ligand still permits polyhistidine-appended proteins and peptides to self-assemble to QDs by spontaneous metal-affinity coordination.[36−40] Our group, along with

a growing number of others, have demonstrated that this simple ratiometric, high-affinity bioconjugation chemistry (K_d ~10^{-9} M) can provide QD-biomolecular assemblies with control over the average number of biologicals attached to each nanocrystal (*i.e.*, valency) along with their relative display orientation. See refs 42 and 43 (and references therein) for detailed reviews of this bioconjugation chemistry and its applications. Moreover, following a simple mixing/assembly step, most such QD conjugates do not require any further purification.

Commercially available paraoxon was used as substrate to assay PTE activity. PTE hydrolyzes the ester-ified phenol group to yield a p-nitrophenol product which strongly absorbs at 405 nm (extinction coefficient ~18 000 M^{-1} cm^{-1}), see Figure 1. Experimentally, PTE was self-assembled to the QDs at increased molar ratios to yield 525/625 QD-(PTE)$_n$ conjugates, substrate was added, and activity was assayed in comparison to equivalent amounts of free PTE controls using a plate reader as described in the Supporting Information. This general format was maintained throughout as different variables such as temperature, presence of competitive inhibitors and viscosity were investigated.

Characterization of Quantum Dot Phosphotriesterase Biocon-jugates. We began by characterizing the QD-PTE bioconjugates that form the basis of these studies. TEM analysis showed the green 525 nm and red 625 nm emitting QDs to have diameters of 4.2 ± 0.5 and 9.2 ± 0.8 nm yielding corresponding hard surface areas of ~60 and 270 nm^2; this corresponds to curvatures (1/radius) of ~0.5 and 0.2 nm^{-1}, respectively.[29] See Figure 2A,B for representative TEM micrographs. The QD-PTE structure was next simulated *in silico* to estimate maximum packing densities and to confirm that
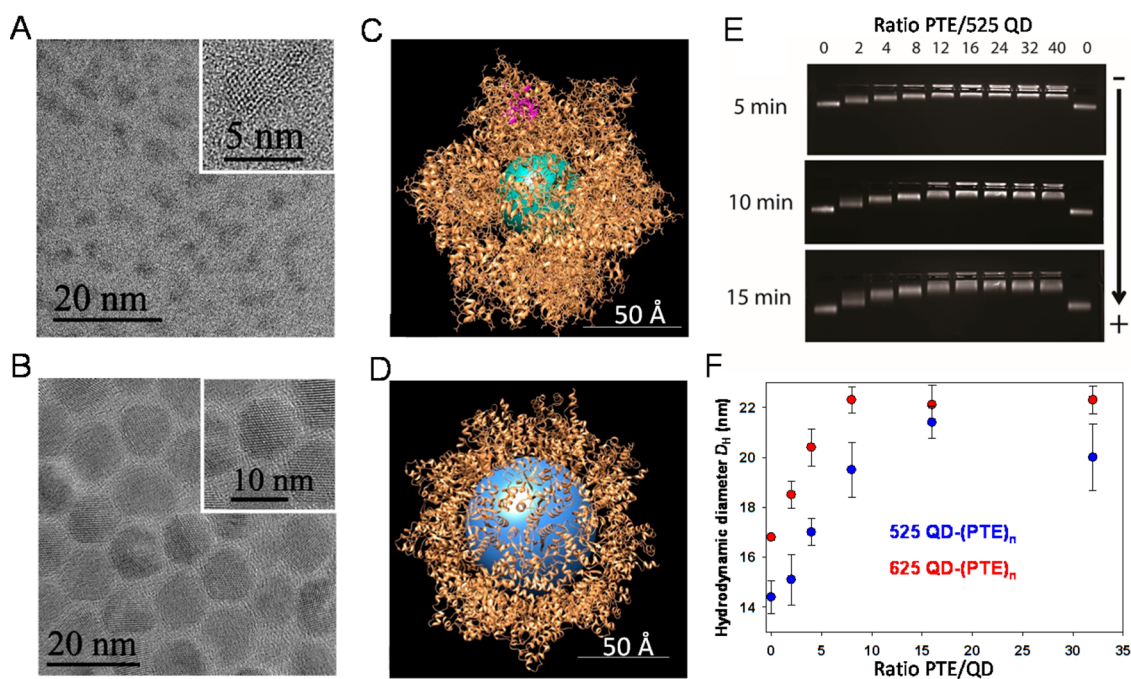
Figure 2. Characterization of QD phosphotriesterase bioconjugates. Representative TEM micrographs of (A) 525 nm emitting and (B) 625 nm emitting CdSe/ZnS QDs with diameters of 4.2 ± 0.5 and 9.2 ± 0.8 nm, respectively. Simulated structures of the (C) 525 QD and (D) 625 QD fully assembled with PTE on the surface as described in the Supporting Information; maximum assembly ratios are estimated at ~13 and 28 PTE/QD, respectively. (E) Agarose gels showing the changes in electrophoretic mobility shifts for the 525 QDs when assembled with the indicated ratios of PTE/QD. (F) Results from DLS analysis plotting the increasing D_H for each QD when assembled with the indicated ratios of PTE.

the enzyme's active site would not be sterically hindered or blocked following assembly. This is accomplished by taking the protein's 3-dimensional structure as estimated by crystallographic coordinates and docking multiple copies to spheres that represent the QDs (Supporting Information). PTE's N-terminal His$_6$ sequence acts as the unique, site-specific attachment point to the QD, and although there is some potential freedom of enzyme movement around this axis, PTE is essentially oriented with the catalytic site fully available on the nanocrystal's outer surface as shown in Figure 2C. This simulation also yields estimated average/maximum loadings of 10/13 and 25/28 PTE for the 525 and 625 nm emitting QDs, respectively.

Electrophoretic mobility shift assays (EMSA) were used to confirm the QD PTE assembly. The gel images in Figure 2E show that as increasing ratios of PTE are assembled on the 525 QDs, their relative mobility shifts in the gel in proportion to the enzyme display density. In this case, no further mobility shifts were noted with ratios greater than 16 loosely corresponding to the predicted assembly maximum of 13. Similar results were noted with the 625 nm QDs, see Supporting Information. Dynamic light scattering (DLS) was also used to monitor increases in the QD-bioconjugate hydrodynamic diameter (D_H) as a function of increasing PTE ratio. A D_H of ~4.4 nm and a diffusion constant of ~96.2 μm^2/s were measured initially for PTE. As seen in Figure 2F (see also Supporting Information Table 1), D_H of the smaller 525 QDs increases proportionally with

PTE addition from an unassembled value of 14.4 to 21.4 nm at a ratio of ~16 PTE, which again we believe reflects maximum packing. The diffusion constant for the 525 QDs decreases from 29.1 to 19.6 μm^2/s at the same ratios. The larger 625 QDs showed similar trends in D_H from an unassembled value of 16.8 to 22.3 nm at a ratio of ~32 PTE with concomitant decreases in the diffusion constant from 24.9 to 18.8 μm^2/s. These are complex colloidal structures consisting of a "hard" central nanocrystal surrounded by a solvated ligand and protein with its own solvation sphere and will thus manifest a D_H that reflects all three contributing entities in a manner that is not easily predicted.[44,45] Cumulatively, the combined structural, electrophoretic and DLS characterization provided good evidence that the PTE assembles to the QDs in a ratiometric manner with controlled orientation. Interestingly, we also note a consistent and repeatable increase in the QD-(PTE)$_n$ D_H of around 5% when in the presence of substrate (data not shown).

Phosphotriesterase Enzymatic Activity. PTE activity both on and off the QDs was next evaluated in identical side-by-side comparative assays. For this, increasing ratios of PTE were assembled on the QDs and these bioconjugates along with equivalent amounts of control enzyme alone were assayed against increasing concentrations of substrate. Figure 3 displays representative plots of the initial rate of p-nitrophenol production for each configuration. Table 1 lists the relevant PTE kinetic parameters obtained from these experiments by fitting
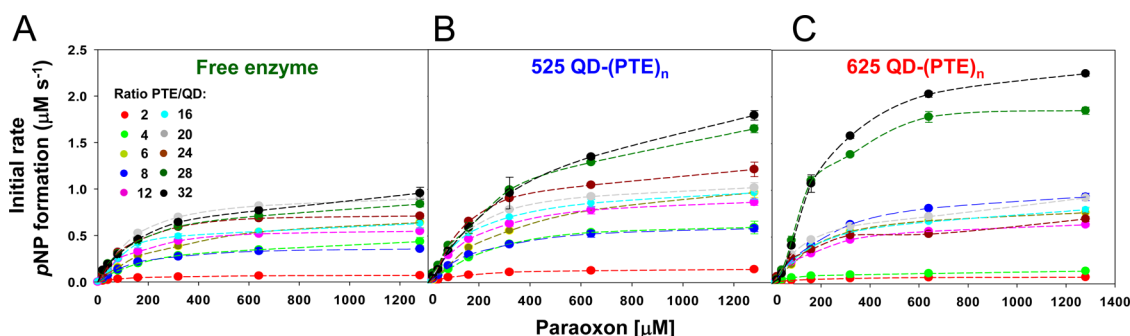
Figure 3. QD phosphotriesterase bioconjugate activity. Initial rates of *p*-nitrophenol product formation for (A) free PTE enzyme, (B) 525 QD-(PTE)$_n$, and (C) 625 QD-(PTE)$_n$ bioconjugates assembled at the indicated ratios when exposed to an increasing concentration of paraoxon substrate. The free PTE enzyme is at the equivalent concentration as that used for the QD-bioconjugates.

**TABLE 1. Estimated PTE Kinetic Parameters on and off QDs**[a]

Ratio of PTE/QD	PTE [nM][b]	V_{max} (μM/s)	k_{cat} (s^{-1})	K_m (μM)	k_{cat} / K_m (mM^{-1}s^{-1})
525 nm QD					
2	2.2	0.16 ± 0.00	71.5 ± 0.8	152 ± 5	470 ± 17
4	4.5	0.75 ± 0.03	166.9 ± 5.7	282 ± 26	591 ± 58
6	6.7	1.30 ± 0.03	193.5 ± 4.9	431 ± 25	448 ± 29
8	8.9	0.69 ± 0.02	77.5 ± 1.9	224 ± 15	344 ± 26
12	13.4	1.00 ± 0.02	74.2 ± 1.1	186 ± 9	398 ± 19
16	17.7	1.11 ± 0.02	62.7 ± 1.2	188 ± 11	333 ± 21
20	22.2	1.18 ± 0.03	53.1 ± 1.1	177 ± 11	300 ± 20
Average:		----	99.9 ± 55.9	235 ± 96	412 ± 100
625 nm QD					
2	2.2	0.08 ± 0.00	37.2 ± 0.6	110 ± 6	338 ± 19
4	4.5	0.15 ± 0.00	34.2 ± 0.4	113 ± 5	301 ± 13
6	6.7	0.78 ± 0.02	116.0 ± 2.4	222 ± 13	523 ± 33
8	8.9	1.03 ± 0.02	115.5 ± 1.8	279 ± 12	414 ± 19
12	13.4	0.92 ± 0.03	68.4 ± 2.2	219 ± 20	312 ± 30
16	17.7	1.20 ± 0.03	67.7 ± 1.4	289 ± 16	234 ± 14
20	22.2	1.02 ± 0.02	46.0 ± 1.1	205 ± 14	225 ± 16
24	26.6	0.74 ± 0.01	27.7 ± 0.8	157 ± 15	176 ± 17
28	31.1	2.33 ± 0.11	74.8 ± 3.7	239 ± 32	314 ± 45
32	35.6	2.95 ± 0.15	83.0 ± 4.2	329 ± 43	253 ± 35
Average:		----	67.0 ± 31.7	216 ± 73	309 ± 91
PTE alone					
Average:	2.2 - 35.6	(low / high range) (0.08 ± 0.0 / 1.08 ± 0.03)	45.5 ± 20.5	160 ± 40	271 ± 68

[a] All assay values are averaged with standard deviations collected from at least 3 independently assembled experiments. Shaded values highlight the unimodal maxima noted for the smaller QDs at low valence along with the bimodal trend seen with the larger QDs. On-QD values are assumed as "apparent" since it is not clear that the MM model is fully valid for NP configurations. [b] PTE concentration in assays.

the MM rate eq (eqs 1 and 2, Materials and Methods). Several trends are noted from this data with the most obvious being that the values do not present a consistent "linear" or correlated pattern as a function of the number of PTEs per QD. In terms of turnover or velocity, the 625 QDs show a V_{max} of ∼3 μM/s at the highest ratio of 32 PTE/QD which is roughly 2.5× the value of ∼1 μM/s observed in the QD-free control at the same PTE concentration. For both QD samples, the catalytic rate (k_{cat}), which is directly reflective of V_{max}, initially rises with increasing enzyme display and then falls off. The 525 QD bioconjugates reach a maximum of ∼194 s^{-1} at a ratio of 6 PTE and then decline to ∼53 s^{-1} at a ratio of 20 *versus* an average value of 46 s^{-1} for the free enzyme control. The 625 QD bioconjugate k_{cat} increases to a

maximum of ∼116 s^{-1} at the same ratio of 6 and then declines to ∼28 s^{-1} at a ratio of 24; however, the rates then start to climb again reaching ∼83 s^{-1} at a ratio of 32. Ratios above the putative packing density were included for the 525 QDs to investigate configurations with enzyme both on and off the QD for potential synergistic effects; these were not observed.

Most importantly, despite some evident experimental error, the data in Table 1 clearly show that putting the PTE on the QDs enhances k_{cat} by about 50% for the larger QDs and by nearly 100% for the smaller QDs on average. Moreover, in the best cases, *e.g.*, the 525 QD with 6 PTEs, the enhancement can be as much as 400%. With regard to K_m, 525 QD-(PTE)$_2$ shows a similar value of 152 μM to the 160 μM noted for PTE
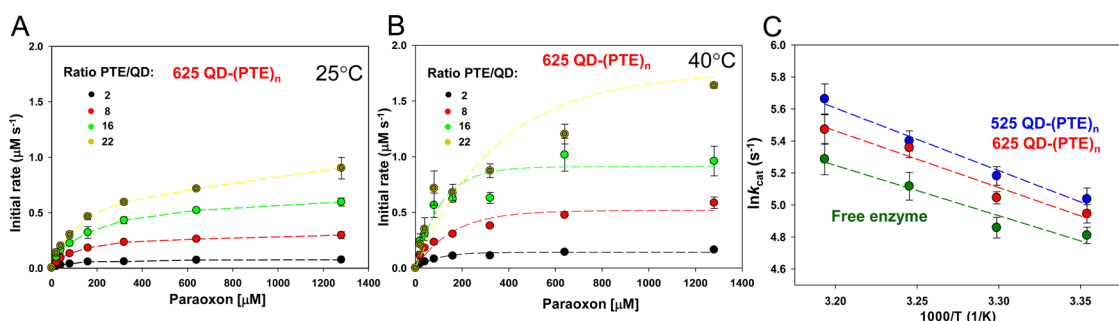
Figure 4. QD phosphotriesterase bioconjugate activity with increasing temperature. Representative initial rates of *p*-nitrophenol product formation for 625-QD-(PTE)$_n$ bioconjugates assembled at the indicated ratios assayed and collected at (A) 25 °C and (B) 40 °C. (C) Arrhenius plot of averaged ln k_{cat} values *versus* inverse temperature (Kelvin) for QD-PTE assemblies and free enzyme. Slopes of the fitted data were -3.9 ± 0.4, -3.5 ± 0.5, and -3.1 ± 0.6 (average = -3.5 ± 0.4) for the 525 QD, 625 QD, and free enzyme, respectively.
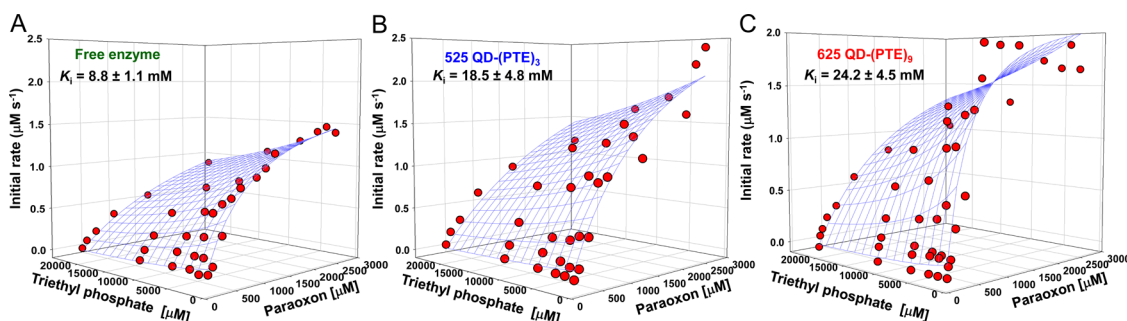
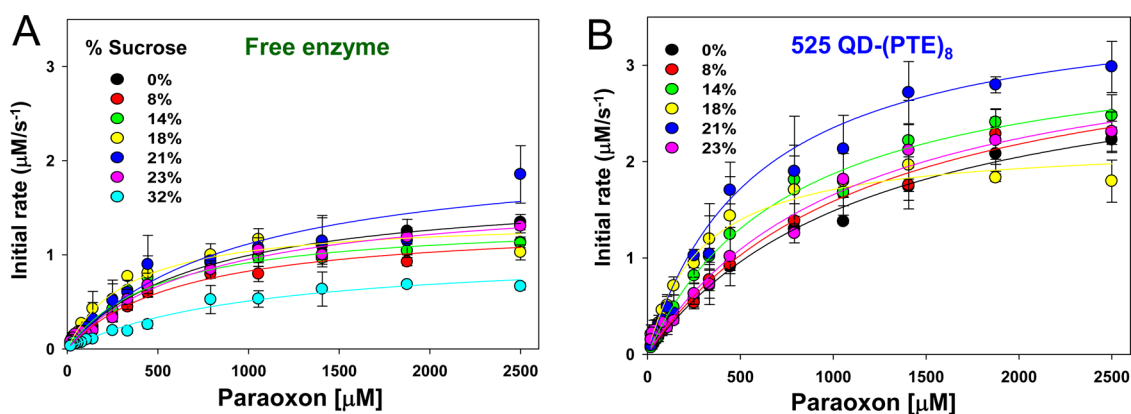**Figure 5. QD phosphotriesterase bioconjugate triethyl phosphate inhibition assays.** Three-dimensional plots of PTE initial rates *versus* increasing paraoxon concentration in the presence of increasing triethyl phosphate inhibitor for (A) free enzyme, (B) 525 QD-(PTE)$_3$, and (C) 625 QD-(PTE)$_9$. Estimated K_i values are included with each.

alone. This then increases to ∼430 μM at a valence of 6 and then drops back to around 180 μM at higher valences. The 625 QD-PTE conjugates show an initial K_m of 110 μM and this increases 3 times to a maxima of 328 for a ratio of 32 PTE per QD. The estimated k_{cat}/K_m values are more insightful as this second-order rate constant reflects the effective efficiency and specificity of each configuration. Overall trends are similar to the k_{cat} values in that an initial climb to a maximum followed by a decrease is seen for both QD systems with the larger QDs again rising and displaying a bimodal response at the highest PTE display ratios. More interesting are that maxima of ∼590 and ∼520 mM^{-1} s^{-1} are seen at the relatively low valencies of 4 and 6 within the 525 and 625 QD bioconjugates, respectively, in comparison to the enzyme-only controls at ∼270 mM^{-1} s^{-1}. Overall, this data provides convincing evidence that the PTE manifests increased kinetic activity and better efficiency when attached to the QDs. To provide more functional insight into the mechanism(s) governing PTE kinetic enhancement at the QD interface, a variety of modified assay formats were next examined.

Modified Assay Formats. *Increased Temperature and Activation Energy.* To probe for changes in the activation energy (E_a) associated with the rate-limiting step of the PTE activity, assays were performed with both QD-PTE conjugates at ratios of 2, 8, 16, and 22 PTE/QD *versus* equivalent amounts of free enzyme over a

temperature range spanning 25−40 °C in 5 °C increments. See Figure 4A,B for representative data from the 625 QD-(PTE)$_n$ collected at the lowest and highest temperatures. The average k_{cat} values at each temperature for the free PTE and QD-mounted PTE are presented in an Arrhenius plot in Figure 4C. It is evident that thermally activated behavior is being seen with an activation energy in all cases of about 37.9 kJ mol^{-1} for the free-enzyme case. This value is also in good agreement (∼5% difference) with that reported by Jackson of 39.9 kJ mol^{-1}.[46] Clearly, there is no significant change in the enzyme's energy of activation when conjugated to the QD confirming that this attachment does not materially affect the PTE itself.

Competitive Inhibition. To look for the presence of more complex or higher order enzyme substrate processes within the on-QD format, assays were also performed in the presence of increasing concentrations of the competitive inhibitor triethyl phosphate (TPE).[47] Figure 5 presents representative 3-D kinetic plots of initial rates as the amount of TPE increases for free enzyme, 525 QD-(PTE)$_3$ and 625 QD-(PTE)$_9$ conjugates, respectively. The control enzyme-only yielded a K_i value of 8.8 mM, while values of 18.5 and 24.2 mM were estimated from the smaller and larger QD data. Averaged K_i values of 18.9 ± 0.8 and 19.6 ± 4.1 mM were estimated from assaying the remaining 525 QD-(PTE)$_{3,6,12}$ and 625 QD-(PTE)$_{9,18,32}$ conjugates,

Figure 6. QD phosphotriesterase bioconjugate activity with increasing viscosity. Plots of PTE initial rates *versus* increasing paraoxon substrate in the presence of increasing sucrose concentration for (A) free enzyme and (B) 525 QD-(PTE)$_8$ conjugates. Percentage sucrose with the corresponding viscosity relative to water (η/η_{H2O}), respectively, are 0% − η = 1, 8−1.251, 14−1.531, 18−1.786, 21−2.027, 23−2.22, 32−3.574.[49]

respectively (data not shown); more inhibitor is functionally required when the enzyme is QD-attached. For comparison purposes, a K_i value of 29.05 ± 4.43 mM was previously reported for PTE interactions with TPE.[48] Subsequent examination of these results in a Dixon format (1/velocity *versus* inhibitor concentration which distinguishes among competitive, uncompetitive and noncompetitive inhibition) confirmed the presence of a competitive inhibition process by convergence of lines above the X axis (data not shown).[11] These assays show that more inhibitor is functionally required when the enzyme is QD-attached confirming the lower K_m values found in the first assay.

Sucrose-Increased Viscosity. Following the work of Raushel, assays were also performed in the presence of increasing concentrations of sucrose so as to study the effect of the microenvironment surrounding the PTE alone or the QD-PTE bioconjugates.[49,50] For PTE in solution, Raushel *et al.* observed decreased turnover rates and argued that they were due to sucrose-associated changes in the microviscosity in the vicinity of the enzyme.[49] The representative plots in Figure 6 compare data for a free-enzyme control (nominally identical to the situation studied by Raushel) with that of the 525 QD-(PTE)$_8$ configurations, with turnover assayed against increasing paraoxon substrate in buffer supplemented with the indicated concentrations of sucrose. The QD-(PTE) ratio of 8 was selected for study as it represents a ratio of slightly less than half the maximum enzyme loadings typically used for the smaller QDs while also encompassing significant apparent increases in k_{cat} for the larger QDs, see Table 1. In all cases, initial rates were substantially affected by the presence of increasing sucrose. The most noteworthy observation is that conjugating PTE on the QD results in a marked change in activity, with free PTE showing a decrease in turnover rate as sucrose is added, whereas in the QD-conjugate case the rates increase.

DISCUSSION AND CONCLUSIONS

When designing formats to probe enzymatic kinetic phenomena at a NP interface, there are several important experimental conditions that should be met. Foremost among these is to have intimate control over the number of enzymes attached per NP along with their relative orientation on the NP. Previous reports examining QD-alkaline phosphatase constructs confirmed that when these key criteria are not met, the resulting NP bioconjugates do not manifest enhanced activity nor even match the activity of the freely diffusing enzyme.[29,51] Consequently, significant efforts including structural modeling along with EMSA and DLS analysis were devoted to confirming that the metal-affinity-coordination-based bioconjugation utilized between the QDs and PTE did indeed provide the requisite control. Here, we focused on PTE hydrolytic activity when attached to *ca.* 4 nm (green 525 nm emission) and 9 nm (red 625 nm emission) diameter QDs and found significant increases in kinetic rates and activity for the QD bioconjugates as compared to controls consisting of the same concentration of enzyme free in solution. For the smaller green QDs, k_{cat} increased to a maximum of ∼4× (193.5 s^{-1}) that of the control (45.5 s^{-1}) at the lower PTE valency of 6 and then decreased with increasing ratios while still remaining higher than the free control values (Table 1). PTE activity on the larger red QDs more than doubled at similar ratios of 6 and 8 and then also dropped off until increasing again at the highest ratios. The k_{cat}/K_m values, in turn, showed similar unimodal and bimodal increases for the smaller and larger QDs, respectively, with a maximum ∼2× increase (590 mM^{-1} s^{-1}) for the smaller QDs at a ratio of 4 PTE *versus* the controls (271 mM^{-1} s^{-1}). Except for the lowest ratios on the larger QDs, the QD-PTE conjugates, by and large, manifest weaker affinity (higher K_m values) than the control samples.

Reports of enhancement of enzymatic activity at a NP interface or when attached to NPs, *i.e.,* turning over

more substrate than equal amounts of enzyme in solution are growing in the literature with examples involving a wide variety of enzymes and NP types/sizes.[19,20] It should be noted, however, that enhancement is not universal and in some cases, including in our own studies,[52] degradation of activity is observed. Different mechanisms have been proposed to explain NP-mediated enhancements. For example, Wu et al. found an improvement in affinity or K_m for lipase adsorption to AuNPs while k_{cat} remained the same.[53] This was supported by an Arrhenius plot indicating a lower activation barrier for the lipase−NP conjugates. In a follow-up study with the same system, catalytic rate was found to increase with decreasing NP size, and this was explained by collision theory and the shielding effect of the NP.[54] This model fails, however, to account for the zero-diameter limit when no NP (and hence no NP shielding) is present and the enzyme performance drops; clearly, the NP itself is necessary for the observed enhancement. Other mechanisms postulated to contribute to enhancement include enzyme conformational changes, NP microenvironment, localized confinement, colocalization, improved substrate trajectories, and even contributions from the unique quantum-confined properties of the NP platforms, see ref 20 and references therein. It seems likely that this diversity in suggested causes is not physical, but rather reflects the poor understanding that currently exists regarding NP enzyme enhancement.

In examining our experimental data for underlying contributors to enhancement, we can first rule out several root causes. In direct contrast to Wu's findings noted above,[53] improvements to the affinity of the enzyme substrate interaction (lower K_m) or lowering of the enzyme's activation energy are clearly not factors; in particular, we find K_m values for PTE are almost always higher (worse affinity) when QD-attached (Table 1) and the activation energy was unchanged between freely diffusing and QD-attached formats (Figure 4). Supporting the negative effects on K_m, we note that the average K_i values for the TPE inhibitor increase ca. 2−3× for the QD-PTE format versus PTE alone (Figure 5). More competitive inhibitor is needed in this format since the enzyme's affinity for it has presumably decreased. From these findings, we conclude that QD enhancements of PTE do not arise from a favorable conformational restructuring of the enzyme itself as this would have manifested in improvements in its affinity.

Seeking more insight into the enzyme's activity, we turn to Raushel's work on understanding PTE catalysis.[30−32,47,49,55] In an elegant set of experiments involving PTE-mediated hydrolysis of various phosphonate esters, Raushel et al.[49] found that k_{cat} decreased exponentially with the pK_a of the substrate's leaving group in keeping with the Brønsted relation, but only when the pK_a was above about 7.5. When the pK_a of a particular substrate was more acidic, k_{cat} no longer

varied implying that the reaction rate was no longer limited by the hydrolysis. Accordingly, a modification of MM kinetics was proposed in which the catalytic step that transforms the enzyme−substrate complex into product was split into two components with first hydrolysis and then product dissociation.[49] This is captured in eq 3 (Materials and Methods section) where the first chemical step is regarded as irreversible and with reaction constant k_{cat}^R, while the physical second step has forward and backward reaction rates that we designate k_2 and k_{-2}, respectively. By this interpretation, phosphonate esters with leaving groups having pK_a's below 7.5 undergo hydrolysis so rapidly that the rate is instead limited by the product dissociation step (see eq 4, Materials and Methods section). For our work, this is of direct interest because it applies to paraoxon whose p-nitrophenol product has a pK_a of 7.14. To probe the dissociation rate limit, Raushel used increasing sucrose concentrations to alter the enzyme's microenvironment by increasing viscosity. Results showed that for paraoxon and similar substrates, k_{cat} decreased in direct proportion to sucrose concentration, confirming that substrate turnover was indeed rate-limited by diffusion-controlled dissociation.[49] As shown in Figure 6, we utilized the same approach to assay PTE hydrolysis of paraoxon when freely diffusing and when attached to the 525 QDs in the presence of increasing sucrose concentration/viscosity. The free PTE turnover rate decreased as sucrose was added just as Raushel found (Figure 6A), but in the QD cases, the rate surprisingly increased (Figure 6B).

Figure 7A plots the normalized k_{cat} values from our sucrose experiments with free PTE together with Raushel's corresponding results,[49] and the good agreement, expected since our PTE is almost an identical homologue,[34] confirms that our free PTE is acting in identical fashion and is thus also rate-limited by product dissociation. The analogous QD data for 525 QD-(PTE)$_8$ bioconjugates is plotted in Figure 7B where we show the normalized values and compare them with the free PTE result from our experiments. A dramatic qualitative difference is seen between the two as we find the k_{cat} values from the QD bioconjugates rise as sucrose is added rather than decrease as in the free PTE case. Whether the reaction scheme in eq 3 is consistent with these measurements is studied in Figures 7C,D where we compare experimental data with simulations based on first-order kinetic equations derived from eq 3 (Supporting Information). Shown in these figures are the initial rates of PTE that is either free in solution (green circles) or the QD-bound form of the 525 QD-(PTE)$_8$ bioconjugate (blue circles). Numerical regression is first used to fit the free PTE data, and the excellent fits obtained (bottom-most red solid curve in each plot) yield two key coefficient values of $k_1 = 0.178$ μM s^{-1} and $k_2 = 145$ s^{-1}. We then look to see if
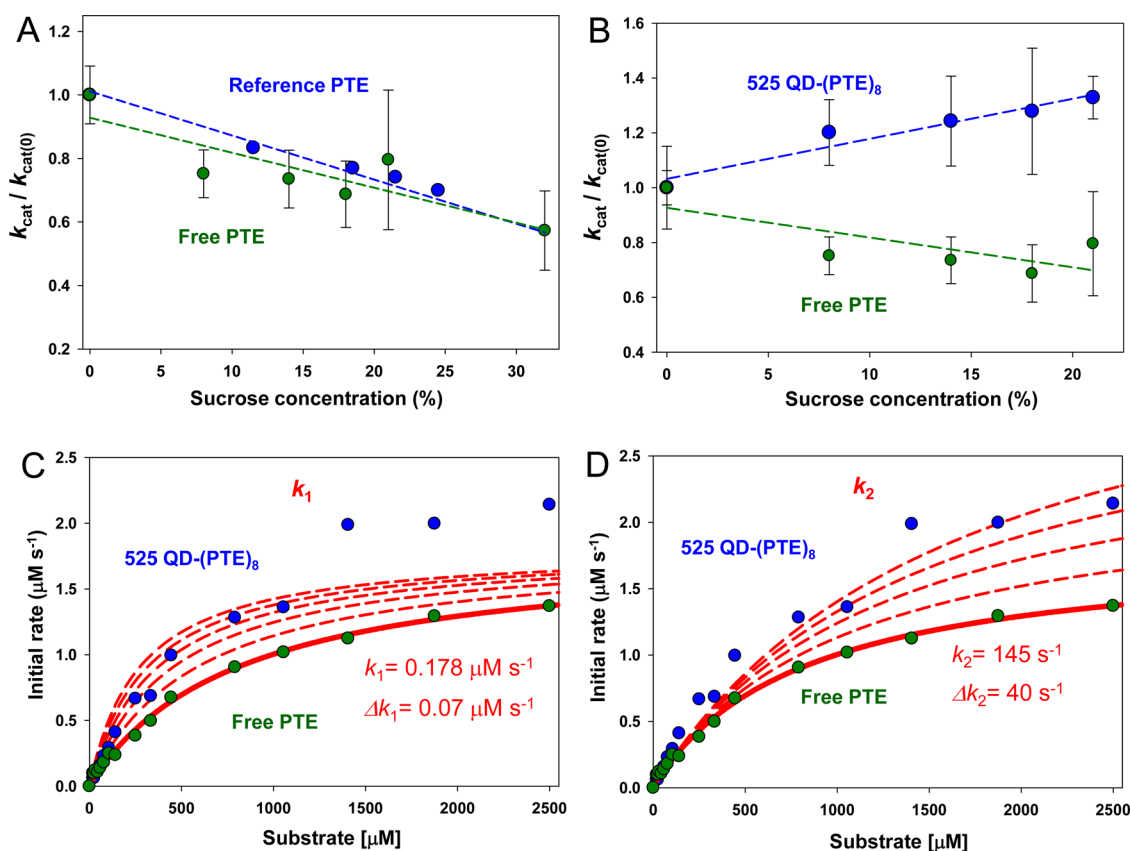
Figure 7. Analysis of phosphotriesterase k_{cat} on and off QD *versus* increasing sucrose concentration. (A) Plots of normalized PTE k_{cat} extracted from ref 48 in blue and current free PTE in green *versus* increasing sucrose concentration. Linear fits of the data are added to each. For the reference data, the fit is extrapolated to the highest sucrose concentration. (B) Plots of normalized PTE k_{cat} values from 525 QD-(PTE)$_8$ conjugates (blue) and equivalent amounts of free PTE (green, same as in plot A) *versus* increasing sucrose concentration. Linear fits added to each data series. (C) Plot comparing the effect of potential changes in k_1 on initial PTE rates. The experimental rates of free PTE (green) and 525 QD-(PTE)$_8$ (blue) *versus* substrate concentration are plotted. An initial k_1 value of 0.178 μM s^{-1} was derived from the experimental value of K_m and a k_{cat} value taken from ref 48 assuming $k_{-1} \ll k_{cat}$. The effect on initial rates of increasing the k_1 value by increments of 0.07 μM s^{-1} is then estimated with the red dashed lines. (D) Plot comparing the effect of potential changes in k_2 on initial PTE rates. The experimental rates of free PTE (green) and 525 QD-(PTE)$_8$ (blue) *versus* substrate concentration are plotted. An initial k_2 value of 145 s^{-1} was derived from the experimental data. The effect on initial rates of increasing the k_2 value by increments of 40 s^{-1} is then estimated with the red dashed lines. Note the overall qualitatively better fit between free and on QD experimental formats when changing k_2 in plot D.

the effect of being on the QD could be explained by simple hypotheses such as that either k_1 (Figure 7C, red dashed curves) or k_2 (Figure 7D, red dashed curves) were modified while all other coefficient values were held fixed. Clearly, Figure 7C shows that with variation in k_1, the simulated on-rate cannot fit the QD data, whereas the good agreement in Figure 7D with k_2 demonstrates that a simple variation in the product dissociation rate could explain the QD effect. This analysis leads us to conclude that PTE attachment at a QD interface effectively alters k_2 constructively allowing for an increase in the apparent activity and the rate of catalysis. Understanding why this anomalous sucrose effect occurs is interesting in itself, but even more important is that in doing so we may well come to better understand how the QD acts to speed up the PTE reaction in the absence of sucrose.

It has long been appreciated that the interface between a NP/colloid and its surrounding aqueous environment is complicated, poorly understood, and the key determinant of the NP's solubility, reactivity and other important physicochemical properties.[56–63] The most important contributor is geometry, with the NP's extremely small radius of curvature typically resulting in little or no crystal faceting, a lack of order in the surface ligands, and more openings for access to water. In addition, there is electrostatics with the formation of a Stern or double layer where localized charges on the NP interact with oppositely charged counterions.[64] The NP surface ligands will also alter the surface microenvironment by virtue of their own interactions with water and with each other, *e.g.*, *via* hydrogen bonding, hydrophilic/hydrophobic interactions, *etc.*[56,58] and the associated solvent restructuring has been suggested to extend to as much as twice the NP diameter.[57] Obviously having enzymes on the surface will further complicate things as they are comparatively large and carry their own charges and

hydration layers. The net effect of all of these interactions is a complex and hard-to-characterize interfacial region that may display ionic and charge gradients, altered pK_a's, partial phase separation, changes in density and viscosity, changes in relative solvation and polarity, and creation of boundary layer(s).[56,58,63] For the present work, we merely acknowledge the complexity of the hydration layer surrounding a QD—enzyme bioconjugate, attempt no general understanding, and confine ourselves to speculating on how this microenvironment might come to substantially increase the enzyme—product dissociation rate.

That our experimental measurements found the PTE activation energy for paraoxon catalysis to be unchanged when situated on the QD suggests that the catalytic mechanism is essentially identical and that the enzyme has not assumed some better structural conformation on the QD. This is consistent with the picture derived from our structural simulations where the polyhistidine sequence that coordinates the enzyme to the QD keeps it available with an outward orientation yet also with some freedom of rotation. This attachment contrasts with a QD-PTE electrostatic assembly method wherein changes to the enzyme structure were noted.[65] Cumulatively, this again leads us to conclude that enhancement arises primarily from a physicochemical change in the QD—enzyme bioconjugate's surrounding localized microenvironment.

This same change to the solvent immediately adjacent to the bioconjugate could also similarly augment k_1, the rate of enzyme—substrate association. Indeed, we observed a slight increase in the QD-PTE bioconjugates D_H in the presence of substrate suggesting that it (or product) was undergoing localized QD accumulation. We note that something similar was also seen with our previous QD—alkaline phosphatase system.[29] The main evidence countering an increase in k_1 along with the poor fit to data seen in Figure 7C is that the acceleration is most evident at high substrate concentrations when the on-rate should be irrelevant. And at lower concentrations, a larger k_1 would be expected to result in a smaller K_m, whereas we see the reverse. Another factor that seems unlikely to play a role is k_{cat}^R, the rate of hydrolysis in the Raushel version of MM kinetics given in eq 3 (Materials and Methods). It was shown by Raushel that this step was not rate-limiting for the PTE—paraoxon reaction when free in solution, with his sucrose experiment being most definitive.[48] That for QD-attached PTE we also observed a sucrose effect, albeit of opposite sign, is an indication that the hydrolysis is still not rate-limiting and that it is the dissociation step that is responsible.

Considering the enzyme—product dissociation, it should be noted that the trends in enhancement seen for both QD sizes in Table 1 are not monotonic and this suggests that the effect is not simple and that several possible mechanisms are operative. The enhancement seen for both QD bioconjugates at the lower ratios are probably attributable to increases in k_2. The smaller magnitude of enhancement seen for the larger QDs may reflect processes like those reported by Wu[53,54] where attenuation may arise from shielding or from bulk repulsion similar to that observed on flat surfaces. More interesting is the bimodal response and especially the second increase in enhancement noted only for the larger QDs at higher valences. Although not as large an enhancement as the first increase at lower ratios, we suggest that the increase here may now arise from a second process, namely avidity and the high localized density of PTE on the larger red QD which has twice the estimated display capacity of the smaller green QDs. As to why k_2 can increase when the PTE is on the QD, one potential hypothesis suggests this was due to a *decrease* in the localized "viscosity" or "friction" felt by the product within the QD's hydration layer or from some other functionally analogous change. The anomalous sucrose effect could then be explained by the action of the sucrose on the hydration layer, *e.g.*, as a result of its osmotic pressure pulling water from the hydration layer. Clarifying these points will certainly require more studies of this system to fully elucidate its localized physicochemical properties. It is important to note that, in general, the ability to characterize the properties of NP-bioconjugates is still significantly hampered by a lack of appropriate analytical techniques and instrumentation.[56,66]

Finally, it is not clear whether the results reported here and the mechanisms that we have speculated about are exclusive to PTE activity at this NP interface or are more reflective of what could be expected for many enzyme—NP constructs if they are optimally assembled. It is noteworthy that experimentally we have observed PTE kinetic enhancement when attached to AuNPs confirming that this phenomena is not exclusive to QDs; these experiments are now underway as part of a follow-up report. Despite the wide variety of postulated causes, the growing number of reports of similar phenomena suggest that there may be some commonality to the underlying contributing mechanisms.[19,20] There have been other reports of attaching PTE to QDs for sensing-based applications; however, no kinetic data was presented precluding a direct comparison.[65,67] Additionally, a reengineered PTE trimer consisting of three monomeric PTEs appended to spontaneously forming collagen-like scaffolds also displayed increased activity when assembled to QDs.[35] In terms of NP—PTE bioconjugate applications, the current results suggest the possibility for developing more robust organophosphate sensors and bioremediation materials; the latter would be even more attractive if the postulate of some localized substrate capture were true.[31] A full understanding of this enhancement phenomena could eventually lead to methods for accelerating other NP—enzyme

bioconjugates. This could help improve many processes where enzymes are currently utilized including in industrial biosynthesis, biofuel production, waste remediation and direct drug applications.

MATERIALS AND METHODS

Quantum Dots and Phosphotriesterase. CdSe/ZnS QDs with emission maxima centered at ∼525 and 625 nm were synthesized and solubilized with dihydrolipoic acid-zwitterionic compact ligand (DHLA-CL4, Figure 1) as described.[36] DHLA-CL4 has a single tertiary amine (pK_a 9.06) which terminates in two alkyl carboxyl groups (pK_a values of 3.29 and 3.93). DHLA-CL4 functionalized QDs demonstrate biocompatibility, high quantum yields, and long-term stability across a broad pH range.[36] Construction of the PTE plasmid and its expression in *E. coli* is detailed in ref 34. A detailed description of the assembly and characterization of QD-PTE bioconjugates along with performing the enzymatic assays can be found in the Supporting Information.

Analysis of PTE Kinetics. The standard approach for analyzing enzyme kinetics is based on the Michaelis−Menten (MM) model in which the reaction steps are typically described as
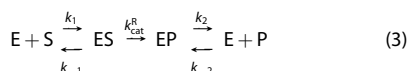
$$E + S \underset{k_{-1}}{\overset{k_1}{\rightleftarrows}} ES \overset{k_{cat}}{\rightarrow} E + P \tag{1}$$

where E, S, P, and ES represent the enzyme, substrate, product, and enzyme−substrate complex, respectively.[11] Assuming linear kinetics with the reaction constants as indicated in eq 1, the initial reaction velocity expression is easily obtained as[68]

$$V \cong \frac{k_{cat}e_0 s_0}{K_m + s_0} \ (i), \quad \text{where} \quad K_m = \frac{k_{-1} + k_{cat}}{k_1} \ (ii) \tag{2}$$

Here e_0 and s_0 are the fixed enzyme and initial substrate concentrations, respectively (with both quantities being per unit total volume). At high substrate concentration, the reaction velocity reaches its maximum, which according to (2*i*) is given by $V_{max} = k_{cat}e_0$. When eq 2 is applied to our initial rate data, *e.g.*, Figure 3, it is found to yield curve-fits that are usually good to excellent. Such agreements do not necessarily imply that the MM reaction scheme (eq 1) is valid or complete, but they do mean that the experimentally derived regression parameters k_{cat} and K_m represent useful quantities for summarizing and comparing experimental data.

The hydrolysis of phosphotriesters by PTE has been studied in great detail by Raushel *et al.*,[30−32,47,49,55] and they argue that a better representation of the reactions involved is[49]

$$E + S \underset{k_{-1}}{\overset{k_1}{\rightleftarrows}} ES \overset{k_{cat}^R}{\rightarrow} EP \underset{k_{-2}}{\overset{k_2}{\rightleftarrows}} E + P \tag{3}$$

where EP represents the enzyme−product complex and the back reaction involving k_{-2} has been made explicit. k_{cat}^R differs from the corresponding MM constant in relating solely to hydrolysis and not also dissociation. When compared with eq 1, the crucial modification of the MM reaction scheme is its separation of the "chemical" hydrolysis step (k_{cat}^R) from the "physical" product release step (k_2). When the k_{-2} process can be neglected, as was assumed implicitly in eq 2, it is readily shown that the initial turnover rate obeys:

$$V \cong \frac{\hat{k}_{cat}e_0 s_0}{\hat{K}_m + s_0} \quad \text{where} \quad \hat{k}_{cat} = \frac{k_{cat}^R k_2}{k_{cat}^R + k_2} \quad \frac{\hat{K}_m}{\hat{k}_{cat}} = \frac{K_m}{k_{cat}^R} \tag{4}$$

The carets in $\hat{k}_{cat}$ and $\hat{K}_m$ differentiate these quantities from those of eq 1 and emphasize that they are experimentally derived and are not necessarily parameters of an underlying kinetic model. That the functional form in eq 4 is identical to that of MM theory (eq 2) means that the curve-fitting involved is the same as with MM kinetics and it is only the meaning of the fitting parameters that is different.

The Arrhenius analysis was based on:

$$\ln(k) = \ln(A) - E_a/RT \tag{5}$$

where k is the rate constant, E_a is the activation energy, R is the gas constant, T is absolute temperature, and A is the frequency or pre-exponential factor.

Conflict of Interest: The authors declare no competing financial interest.

Supporting Information Available: Includes additional methods and supporting experimental results. The Supporting Information is available free of charge on the ACS Publications website at DOI: 10.1021/acsnano.5b03459.

REFERENCES AND NOTES

1. Keasling, J. D. Manufacturing Molecules Through Metabolic Engineering. *Science* **2010**, *330*, 1355–1358.
2. Runguphan, W.; Keasling, J. D. Metabolic Engineering of Saccharomyces cerevisiae for Production of Fatty Acid-Derived Biofuels and Chemicals. *Metab. Eng.* **2014**, *21*, 103–113.
3. Correa, R. C. G.; Rhoden, S. A.; Mota, T. R.; Azevedo, J. L.; Pamphile, J. A.; de Souza, C. G. M.; Polizeli, M.; Bracht, A.; Peralta, R. M. Endophytic Fungi: Expanding the Arsenal of Industrial Enzyme Producers. *J. Ind. Microbiol. Biotechnol.* **2014**, *41*, 1467–1478.
4. Borodina, I.; Nielsen, J. Advances in Metabolic Engineering of Yeast Saccharomyces cerevisiae for Production of Chemicals. *Biotechnol. J.* **2014**, *9*, 609–620.
5. Hofbauer, S.; Schaffner, I.; Furtmuller, P. G.; Obinger, C. Chlorite Dismutases - A Heme Enzyme Family for Use in Bioremediation and Generation of Molecular Oxygen. *Biotechnol. J.* **2014**, *9*, 461–473.
6. Nafissi, N.; Slavcev, R. Bacteriophage Recombination Systems and Biotechnical Applications. *Appl. Microbiol. Biotechnol.* **2014**, *98* (7), 2841–2851.
7. Chellapandi, P. Structural, Functional and Therapeutic Aspects of Snake Venom Metalloproteinases. *Mini-Rev. Org. Chem.* **2014**, *11*, 28–44.
8. Liu, F.; Banta, S.; Chen, W. Functional Assembly of a Multi-Enzyme Methanol Oxidation Cascade on a Surface-Displayed Trifunctional Scaffold for Enhanced NADH Production. *Chem. Commun.* **2013**, *49*, 3766–3768.
9. Payne, C. M.; Knott, B. C.; Mayes, H. B.; Hansson, H.; Himmel, M. E.; Sandgren, M.; Ståhlberg, J.; Beckham, G. T. Fungal Cellulases. *Chem. Rev.* **2015**, *115*, 1308–1448.
10. Bornscheuer, U. T.; Huisman, G. W.; Kazlauskas, R. J.; Lutz, S.; Moore, J. C.; Robins, K. Engineering the Third Wave of Biocatalysis. *Nature* **2012**, *485*, 185–194.
11. Cornish-Bowden, A. *Fundamentals of Enzyme Kinetics*; John Wiley & Sons: New York, 2013.
12. Paap, S. M.; West, T. H.; Manley, D. K.; Steen, E. J.; Beller, H. R.; Keasling, J. D.; Dibble, D. C.; Chang, S. Y.; Simmons, B. A. Biochemical Production of Ethanol and Fatty Acid Ethyl Esters from Switchgrass: A Comparative Analysis of Environmental and Economic Performance. *Biomass Bioenergy* **2013**, *49*, 49–62.
13. Zhang, F. Z.; Rodriguez, S.; Keasling, J. D. Metabolic Engineering of Microbial Pathways for Advanced Biofuels Production. *Curr. Opin. Biotechnol.* **2011**, *22*, 775–783.
14. Butterfield, D. A.; Bhattacharyya, D.; Daunert, S.; Bachas, L. Catalytic Biofunctional Membranes Containing Site-Specifically

Immobilized Enzyme Arrays: A Review. *J. Membr. Sci.* **2001**, *181*, 29–37.

15. Rao, S. V.; Anderson, K. W.; Bachas, L. G. Oriented Immobilization of Proteins. *Microchim. Acta* **1998**, *128*, 127–143.

16. Jesionowski, T.; Zdarta, J.; Krajewska, B. Enzyme Immobilization by Adsorption: A Review. *Adsorption* **2014**, *20*, 801–821.

17. de Poulpiquet, A.; Ciaccafava, A.; Lojou, E. New Trends in Enzyme Immobilization at Nanostructured Interfaces for Efficient Electrocatalysis in Biofuel Cells. *Electrochim. Acta* **2014**, *126*, 104–114.

18. Sapsford, K. E.; Algar, W. R.; Berti, L.; Gemmill, K. B.; Casey, B. J.; Oh, E.; Stewart, M. H.; Medintz, I. L. Functionalizing Nanoparticles with Biological Molecules: Developing Chemistries that Facilitate Nanotechnology. *Chem. Rev.* **2013**, *113*, 1904–2074.

19. Ansari, S. A.; Husain, Q. Potential Applications of EnzymesI on/in Nano Materials: A Review. *Biotechnol. Adv.* **2012**, *30*, 512–523.

20. Johnson, B. J.; Russ Algar, W.; Malanoski, A. P.; Ancona, M. G.; Medintz, I. L. Understanding Enzymatic Acceleration at Nanoparticle Interfaces: Approaches and Challenges. *Nano Today* **2014**, *9*, 102–131.

21. Konwarh, R.; Karak, N.; Rai, S. K.; Mukherjee, A. K. Polymer-Assisted Iron Oxide Magnetic Nanoparticle Immobilized Keratinase. *Nanotechnology* **2009**, *20*, 225107.

22. Ardao, I.; Comenge, J.; Benaiges, M. D.; Álvaro, G.; Puntes, V. F. Rational Nanoconjugation Improves Biocatalytic Performance of Enzymes: Aldol Addition Catalyzed by Immobilized Rhamnulose-1-Phosphate Aldolase. *Langmuir* **2012**, *28*, 6461–6467.

23. Palocci, C.; Chronopoulou, L.; Venditti, I.; Cernia, E.; Diociaiuti, M.; Fratoddi, I.; Russo, M. V. Lipolytic Enzymes with Improved Activity and Selectivity Upon Adsorption on Polymeric Nanoparticles. *Biomacromolecules* **2007**, *8*, 3047–3053.

24. Noble, G. T.; Craven, F. L.; Voglmeir, J.; Sardzik, R.; Flitsch, S. L.; Webb, S. J. Accelerated Enzymatic Galactosylation of N-Acetylglucosaminolipids in Lipid Microdomains. *J. Am. Chem. Soc.* **2012**, *134*, 13010–13017.

25. Prigodich, A. E.; Alhasan, A. H.; Mirkin, C. A. Selective Enhancement of Nucleases by Polyvalent DNA-Functionalized Gold Nanoparticles. *J. Am. Chem. Soc.* **2011**, *133*, 2120–2123.

26. Lupoi, J. S.; Smith, E. A. Evaluation of Nanoparticle-Immobilized Cellulase for Improved Ethanol Yield in Simultaneous Saccharification and Fermentation Reactions. *Biotechnol. Bioeng.* **2011**, *108*, 2835–2843.

27. Algar, W. R.; Malonoski, A.; Deschamps, J. R.; Blanco-Canosa, J. B.; Susumu, K.; Stewart, M. H.; Johnson, B. J.; Dawson, P. E.; Medintz, I. L. Proteolytic Activity at Quantum Dot-Conjugates: Kinetic Analysis Reveals Enhanced Enzyme Activity and Localized Interfacial "Hopping. *Nano Lett.* **2012**, *12*, 3793–3802.

28. Wu, M.; Algar, W. R. Acceleration of Proteolytic Activity Associated with Selection of Thiol Ligand Coatings on Quantum Dots. *ACS Appl. Mater. Interfaces* **2015**, *7*, 2535–2545.

29. Claussen, J. C.; Malanoski, A.; Breger, J. C.; Oh, E.; Walper, S. A.; Susumu, K.; Goswami, R.; Deschamps, J. R.; Medintz, I. L. Probing the Enzymatic Activity of Alkaline Phosphatase Within Quantum Dot Bioconjugates. *J. Phys. Chem. C* **2015**, *119*, 2208–2221.

30. Bigley, A. N.; Raushel, F. M. Catalytic Mechanisms for Phosphotriesterases. *Biochim. Biophys. Acta, Proteins Proteomics* **2013**, *1834*, 443–453.

31. Tsai, P. C.; Fox, N.; Bigley, A. N.; Harvey, S. P.; Barondeau, D. P.; Raushel, F. M. Enzymes for the Homeland Defense: Optimizing Phosphotriesterase for the Hydrolysis of Organophosphate Nerve Agents. *Biochemistry* **2012**, *51*, 6463–6475.

32. Donarski, W. J.; Dumas, D. P.; Heitmeyer, D. P.; Lewis, V. E.; Raushel, F. M. Structure Activity Relationships in the Hydrolysis of Substrates by the Phosphotriesterase from Pseudomonas-Diminuta. *Biochemistry* **1989**, *28*, 4650–4655.

33. Hong, S.-B.; Raushel, F. M. Metal-Substrate Interactions Facilitate the Catalytic Activity of the Bacterial Phosphotriesterase. *Biochemistry* **1996**, *35*, 10904–10912.

34. Susumu, K.; Oh, E.; Delehanty, J. B.; Pinaud, F.; Gemmill, K. B.; Walper, S.; Breger, J.; Schroeder, M. J.; Stewart, M. H.; Jain, V.; et al. A New Family of Pyridine-Appended Multidentate Polymers As Hydrophilic Surface Ligands for Preparing Stable Biocompatible Quantum Dots. *Chem. Mater.* **2014**, *26*, 5327–5344.

35. Breger, J. C.; Walper, S. A.; Oh, E.; Susumu, K.; Stewart, M. H.; Deschamps, J. R.; Medintz, I. L. Quantum Dot Display Enhances Activity of a Phosphotriesterase Trimer. *Chem. Commun.* **2015**, *51*, 6403–6406.

36. Susumu, K.; Oh, E.; Delehanty, J. B.; Blanco-Canosa, J. B.; Johnson, B. J.; Jain, V.; Hervey, W. J.; Algar, W. R.; Boeneman, K.; Dawson, P. E.; et al. Multifunctional Compact Zwitterionic Ligands for Preparing Robust Biocompatible Semiconductor Quantum Dots and Gold Nanoparticles. *J. Am. Chem. Soc.* **2011**, *133*, 9480–9496.

37. Breger, J. C.; Sapsford, K. E.; Ganek, J.; Susumu, K.; Stewart, M. H.; Medintz, I. L. Detecting Kallikrein Proteolytic Activity with Peptide-Quantum Dot Nanosensors. *ACS Appl. Mater. Interfaces* **2014**, *6*, 11529–11535.

38. Walters, R.; Kraig, R. P.; Medintz, I.; Delehanty, J. B.; Stewart, M. H.; Susumu, K.; Huston, A. L.; Dawson, P. E.; Dawson, G. Nanoparticle Targeting to Neurons in a Rat Hippocampal Slice Culture Model. *ASN Neuro* **2012**, *4*, 383–392.

39. Boeneman Gemmill, K.; Deschamps, J. R.; Delehanty, J. B.; Susumu, K.; Stewart, M. H.; Glaven, R. H.; Anderson, G. P.; Goldman, E. R.; Huston, A. L.; Medintz, I. L. Optimizing Protein Coordination to Quantum Dots with Designer Peptidyl Linkers. *Bioconjugate Chem.* **2013**, *24*, 269–281.

40. Boeneman; Gemmill, K.; Delehanty, J. B.; Blanco-Canosa, J.; Susumu, K.; Stewart, M. H.; Oh, E.; Huston, A. L.; Dawson, G.; Ingale, S.; Walters, R.; et al. Selecting Improved Peptidyl Motifs for Cytosolic Delivery of Disparate Protein and Nanoparticle Materials. *ACS Nano* **2013**, *7*, 3778–3796.

41. Agarwal, R.; Domowicz, M.; Schwartz, N.; Henry, J.; Medintz, I. L.; Delehanty, J. B.; Stewart, M.; Susumu, K.; Huston, A.; Deschamps, J. R.; et al. Delivery and Tracking of Quantum Dot Peptide Bioconjugates in an Intact Developing Avian Brain. *ACS Chem. Neurosci.* **2015**, *6*, 494–504.

42. Blanco-Canosa, J. B.; Wu, M.; Susumu, K.; Petryayeva, E.; Jennings, T. L.; Dawson, P. E.; Algar, W. R.; Medintz, I. L. Recent progress in the Bioconjugation of Quantum Dots. *Coord. Chem. Rev.* **2014**, *263-264*, 101–137.

43. Nagy, A.; Boeneman; Gemmill, K.; Delehanty, J. B.; Medintz, I. L.; Sapsford, K. E. Peptide-Functionalized Quantum Dot Biosensors. *IEEE J. Sel. Top. Quantum Electron.* **2014**, *20*, 6900512.

44. Pons, T.; Uyeda, H. T.; Medintz, I. L.; Mattoussi, H. Hydrodynamic Dimensions, Electrophoretic Mobility, and Stability of Hydrophilic Quantum Dots. *J. Phys. Chem. B* **2006**, *110*, 20308–20316.

45. Oh, E.; Fatemi, F. K.; Currie, M.; Delehanty, J. B.; Pons, T.; Fragola, A.; Leveque-Fort, S.; Goswami, R.; Susumu, K.; Huston, A. L.; et al. PEGylated Luminescent Gold Nanoclusters: Synthesis, Characterization, Bioconjugation, and Application to One- and Two-Photon Cellular Imaging. *Particle & Particle Syst. Charact.* **2013**, *30*, 453–466.

46. Jackson, C. J.; Foo, J. L.; Tokuriki, N.; Afriat, L.; Carr, P. D.; Kim, H. K.; Schenk, G.; Tawfik, D. S.; Ollis, D. L. Conformational Sampling, Catalysis, and Evolution of the Bacterial Phosphotriesterase. *Proc. Natl. Acad. Sci. U. S. A.* **2009**, *106*, 21631–21636.

47. Benning, M. M.; Hong, S. B.; Raushel, F. M.; Holden, H. M. The Binding of Substrate Analogs to Phosphotriesterase. *J. Biol. Chem.* **2000**, *275*, 30556–30560.

48. Larsen, S. D. *Structure, Mechanism, and Evolution of Organophosphorus Hydrolase from Deinococcus radiodurans*; University of Illinois at Chicago: Chicago, IL, 2008.

49. Caldwell, S. R.; Newcomb, J. R.; Schlecht, K. A.; Raushel, F. M. Limits of Diffusion in the Hydrolysis of Substrates by the Phosphotriesterase from Pseudomonas-Diminuta. *Biochemistry* **1991**, *30* (30), 7438–7444.

50. Swindells, J. F.; Snyder, C. F.; Hardy, R. C.; Golden, P. E. *Viscosities of Sucrose Solutions at Various Temperatures: Tables of Recalculated Values*; National Bureau of Standards, U.S. Government Printing Office: Washington, DC, 1958; Supplement to National Bureau of Standards Circular 440.

51. Iyer, A.; Chandra, A.; Swaminathan, R. Hydrolytic Enzymes Conjugated to Quantum Dots Mostly Retain Whole Catalytic Activity. *Biochim. Biophys. Acta, Gen. Subj.* **2014**, *1840*, 2935–2943.

52. Diaz, S. A.; Malanoski, A.; Susumu, K.; Hofele, R. V.; Oh, E.; Medintz, I. L. Probing the Kinetics of Quantum Dot-Based Proteolytic Sensors. *Anal. Bioanal. Chem.* **2015**, DOI: 10.1007/s00216-015-8892-y.

53. Wu, C. S.; Wu, C. T.; Yang, Y. S.; Ko, F. H. An Enzymatic Kinetics Investigation Into the Significantly Enhanced Activity of Functionalized Gold Nanoparticles. *Chem. Commun.* **2008**, *42*, 5327–5329.

54. Wu, C.-S.; Lee, C.-C.; Wu, C.-T.; Yang, Y.-S.; Ko, F.-H. Size-Modulated Catalytic Activity of Enzyme−Nanoparticle Conjugates: A Combined Kinetic and Theoretical Study. *Chem. Commun.* **2011**, *47*, 7446–7448.

55. Benning, M. M.; Kuo, J. M.; Raushel, F. M.; Holden, H. M. Three-Dimensional Structure of the Binuclear Metal Center of Phosphotriesterase. *Biochemistry* **1995**, *34*, 7973–7978.

56. Pfeiffer, P.; Rehbock, C.; Huhn, D.; Carrillo-Carrion, C.; de Aberasturi, D. J.; Merk, V.; Barcikowski, S.; Parak, W. J. Interaction of Colloidal Nanoparticles with Their Local Environment: The (Ionic) Nanoenvironment Around Nanoparticles is Different From Bulk and Determines the Physico-Chemical Properties of the Nanoparticles. *J. R. Soc., Interface* **2014**, *11*, 20130931.

57. Zobel, M.; Neder, R. B.; Kimber, S. A. J. Universal Solvent Restructuring Induced by Colloidal Nanoparticles. *Science* **2015**, *347*, 292–294.

58. Zhang, F.; Ali, Z.; Amin, F.; Feltz, A.; Oheim, M.; Parak, W. J. Ion and pH Sensing with Colloidal Nanoparticles: Influence of Surface Charge on Sensing and Colloidal Properties. *ChemPhysChem* **2010**, *11*, 730–735.

59. Zhou, J. F.; Ralston, J.; Sedev, R.; Beattie, D. A. Functionalized Gold Nanoparticles: Synthesis, Structure and Colloid Stability. *J. Colloid Interface Sci.* **2009**, *331*, 251–262.

60. Iijima, M.; Kamiya, H. Surface Modification for Improving the Stability of Nanoparticles in Liquid Media. *KONA* **2009**, *27*, 119–129.

61. Narayanan, R.; El-Sayed, M. A. Catalysis with Transition Metal Nanoparticles in Colloidal Solution: Nanoparticle Shape Dependence and Stability. *J. Phys. Chem. B* **2005**, *109*, 12663–12676.

62. Hiemenz, P. C.; Rajagopalan, R. *Principles of Colloid and Surface Chemistry*, 3rd ed.; CRC Press: Boca Raton, FL, 1997.

63. Talbert, J. N.; Goddard, J. M. Enzymes on Material Surfaces. *Colloids Surf., B* **2012**, *93*, 8–19.

64. Ridley, M. K.; Machesky, M. L.; Kubicki, J. D. Anatase Nanoparticle Surface Reactivity in NaCl Media: A CD-MUSIC Model Interpretation of Combined Experimental and Density Functional Theory Studies. *Langmuir* **2013**, *29*, 8572–8583.

65. Ji, X.; Zheng, J.; Xu, J.; Rastogi, V. K.; Cheng, T.-C.; DeFrank, J. J.; Leblanc, R. M. (CdSe)ZnS Quantum Dots and Organophosphorus Hydrolase Bioconjugate as Biosensors for Detection of Paraoxon. *J. Phys. Chem. B* **2005**, *109*, 3793–3799.

66. Sapsford, K. E.; Tyner, K. M.; Dair, B. J.; Deschamps, J. R.; Medintz, I. L. Analyzing Nanomaterial Bioconjugates: A Review of Current and Emerging Purification and Characterization Techniques. *Anal. Chem.* **2011**, *83*, 4453–4488.

67. Du, D.; Chen, W. J.; Zhang, W. Y.; Liu, D. L.; Li, H. B.; Lin, Y. H. Covalent Coupling of Organophosphorus Hydrolase Loaded Quantum Dots to Carbon Nanotube/Au Nanocomposite for Enhanced Detection of Methyl Parathion. *Biosens. Bioelectron.* **2010**, *25*, 1370–1375.

68. Segel, I. H. *Enzyme Kinetics: Behavior and Analysis of Rapid Equilibrium and Steady-State Enzyme Systems*, 1st ed.; Wiley-Interscience: New York, 1992.